water

Article

Study on Flow Characteristics of Francis Turbine Based on Large-Eddy Simulation

Tianyu Xu [1], Quanjie Cheng [1], Changjiang Lin [1], Qiuyue Yu [2,*] and Xiucheng Hu [3,*]

1 School of Hydraulic and Electric Power, Heilongjiang University, Harbin 150080, China; 2021007@hlju.edu.cn (T.X.); 15848607008@163.com (Q.C.); linchangjiang0423@163.com (C.L.)
2 Heilongjiang Academy of Black Soil Conservation and Utilization, Harbin 150086, China
3 Yunnan Huadian Jinsha River Hydropower Development Co., Ltd., Kunming 650228, China
* Correspondence: 18845572099@163.com (Q.Y.); huxc2007@icloud.com (X.H.)

Abstract: The research object was a Francis turbine, and the working conditions at 100%, 75%, 50%, 25%, and 1% opening were determined by the opening size of the guide vane. Large-Eddy Simulation (LES) was adopted as a turbulence model method to conduct three-dimensional unsteady turbulent numerical simulation of the entire flow channel of a Francis turbine, and the flow situation of various parts of the turbine under different working conditions was obtained. The flow characteristics of each component under different working conditions were analyzed, and the hydraulic performance of each part was evaluated. The factors that affected the stability of hydraulic turbines were identified, and their formation mechanisms and evolution laws were explored. The results show that the guide vane placement angle was reasonable in the guide vane area, and the hydraulic performance was fine. The impact on the stability of the hydraulic turbine was small. Further research showed that the hydraulic performance was poor in the runner area, and there were flow separation and detachment phenomena in the flow field. This created a channel vortex in the runner blade channel. The channel vortex promoted the lateral flow of water and had a significant impact on the stability of the hydraulic turbine. The diffusion section of the draft tube can dissipate most of the kinetic energy of the water flow in the draft tube area, and it had a good energy dissipation effect. However, the was a large pressure difference between the upper and lower regions of the diffusion section, and it generated a backflow phenomenon. It created vortex structures in the draft tube, and the stability of the hydraulic turbine was greatly affected.

Keywords: Francis turbine; guide vane opening; flow characteristic; numerical simulation

check for updates

Citation: Xu, T.; Cheng, Q.; Lin, C.; Yu, Q.; Hu, X. Study on Flow Characteristics of Francis Turbine Based on Large-Eddy Simulation. *Water* **2023**, *15*, 3372. https://doi.org/10.3390/w15193372

Academic Editors: Mohammadreza Mohammadi, Moona Mohammadi and Nigel Wright

Received: 8 August 2023
Revised: 18 September 2023
Accepted: 25 September 2023
Published: 26 September 2023

1. Introduction

Hydropower is a clean, renewable energy source and can be developed commercially on a large scale [1]. Due to the increasing importance of renewable energy, the integration of renewable energy requires greater flexibility in the power grid. Hydroelectric units have to frequently change working conditions to cope with fluctuations in grid load, and this means that hydroelectric units will have more time under partial load conditions [2]. The turbine is the core equipment of the hydropower unit, and the most common type of turbine is the Francis turbine. It converts water energy into rotational power by driving a generator to generate electrical energy. Francis turbines are widely used in hydropower plants, power stations, and other places. Compared with other turbines, Francis turbines have a wider operating range, higher efficiency, and smaller size. The internal flow field of a Francis turbine will inevitably generate vortex structures and pressure pulsations during the transition process. The internal vortex structure of a hydraulic turbine not only generates noise and vibration but also reduces the output power of the turbine, which can affect its stability [3,4]. So far, the mechanism and influencing factors of the internal vortex structure of hydraulic turbines have not been fully understood under the influence of complex internal flow fields. It is important to study the flow characteristics of the internal flow field of hydraulic turbines to improve their stability.

With the development of computational fluid dynamics (CFD), numerical simulation has become one of the main methods to study hydraulic turbines. Many scholars have studied the factors affecting turbine vibration, and the vortex rope in draft tubes was identified as the main cause of turbine vibration [5–8]. There are also some scholars who believe that the channel vortex inside the runner also affected the vibration of the turbine [9–12]. The flow characteristics within the draft tube and runner are intricate, and there is no consistent conclusion on the formation mechanism of the channel vortex and the vortex rope in the draft tube [13]. Liu et al. [14] suggested that the larger incidence angle between the inflow angle and the blade angle on the leading edge of the runner was the formation factor of the channel vortex. Liu et al. [15] believed that the channel vortex was caused by the reverse flow of water in the draft tube. Zhang et al. [16] considered the unsteady vortex flow in the straight cone section as the main cause of the vortex rope in the draft tube. In recent years, many scholars have researched measures to reduce the vibration of hydraulic turbines. Tran et al. [17] improved the cavitation performance of a hydraulic turbine by adding splitter blades in the runner blade channel. Sun et al. [18] found that injecting air into the runner blade channel can significantly alleviate the development of channel vortices. The vibration of hydraulic turbines can be effectively reduced by adding baffle at the draft tube or lengthening the drainage cone [19,20].

When a hydraulic turbine is in nonoptimal working conditions, vibration is inevitable. Guo et al. [21] found that as the opening of the guide vanes decreased, the cavitation phenomenon in the runner increased, and local high-pressure or negative pressure areas appeared on the blades. Zhou [22] concluded that the increase in the guide vane opening helped to reduce the pressure acting on the runner blades, and the backflow was more likely to occur at the end of the runner blades. Kan et al. [23] found turbulence in the flow pattern within the runner and uneven stress distribution on the blades under low flow conditions. Ji et al. [24] found that the vortex structure inside the draft tube became clear when the opening of the guide vanes increased. This improved the performance of the hydraulic turbine.

So far, many scholars have analyzed the internal vortex structure of Francis turbines and the evolution of flow characteristics. However, the initial position of the vortex channel has still not been accurately located, and the evolutionary pattern of the vortex structure in the draft tube area is not known. Further exploring the formation mechanism of internal vortex structures in hydraulic turbines and analyzing their impact on turbine vibration and cavitation is of great significance for improving the stability of hydraulic turbines. In this paper, the computational fluid dynamics method was used to study a prototype Francis turbine. It can (1) compare the flow characteristics of various parts of the hydraulic turbine under different working conditions, (2) evaluate the flow performance of each part of the hydraulic turbine, (3) explore the factors that affect the stability of hydraulic turbines, and (4) analyze their formation mechanism and evolution law.

2. Calculation Method

2.1. Model Construction

The research object was a Francis turbine. The three-dimensional fluid domain model of the full-flow channel of the Francis turbine is shown in Figure 1.

The rated head of the water turbine was 200 m. The rated speed was 300 rpm, and the opening of the guide vanes under the rated working condition was 23°. The basic parameters of the water turbine are shown in Table 1.

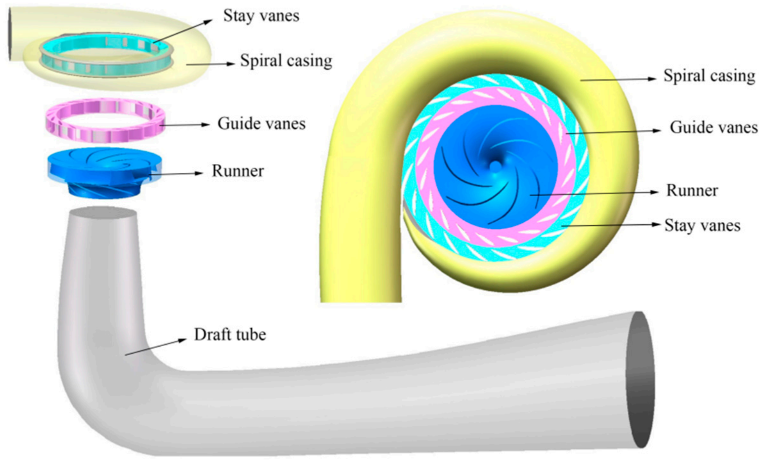

Figure 1. Three-dimensional Model of the Full-Flow Channel of a Hydraulic Turbine.

Table 1. Basic Parameters of Hydraulic Turbines.

Parameters	Value
Rated head Hr (m)	200
Rated flow rate of hydraulic turbine under working conditions Q_r (m^3/s)	148.37
Rated speed (rpm)	300
Number of runner blades Z_1	7
Number of stay vanes Z_c	20
Number of guide vanes Z_0	20
Rated hydraulic turbine working condition guide vane opening (°)	23
Diameter of spiral casing inlet (m)	3.20
Diameter of runner D_1 (m)	4.68
Diameter of guide vanes circle D_0 (m)	5.60
Guide vane height (m)	0.66

2.2. Grid Division and Independence Test

Grid division was the most important step in the numerical simulation of hydraulic turbines, and the quality of the grid directly affected the accuracy of the results. In this paper, the spiral casing and runner were divided nonstructurally, and the stay vane, guide vane, and draft tube were divided structurally. The Schemes A, B, and C were designed for grid independence testing. The corresponding grid numbers for schemes A, B, and C were 3 million, 5 million, and 8 million, respectively. The characteristics of different grids is summarized in Table 2. The skewness was considered to be better closer to 0, while orthogonal quality was considered to be better closer to 1. From Table 2, it can be seen that the grid quality of Scheme B was better. The average pressure value of the runner blade pressure surface and the average flow velocity value of the turbine outlet section were compared and analyzed. As shown in Figure 2, the flow velocity was 19 m/s and the pressure was 1.43×10^6 pa when the number of grids was 3 million. The flow velocity was 23 m/s and the pressure was 1.56×10^6 pa when the number of grids was 5 million. The flow velocity was 24 m/s and the pressure was 1.60×10^6 pa when the number of grids was 8 million. The difference in flow velocity and pressure between 5 million and 8 million grids was 4.2% and 2.5%, respectively. This means that the sensitivity of the simulation results to the number of grids decreased. From the perspective of computational efficiency and cost, this paper selected scheme B as the computational grid. In order to verify the rationality of the results near the wall, the y^+ value near the wall was measured. The average y^+ value on the blade wall of Scheme B was 38. According to [25], a y^+ value of less than 50 can also achieve good results when using Large-Eddy Simulation. The results near the wall can be considered reasonable. Figure 3 shows the details of grid division.

Table 2. The characteristics of different schemes.

	Orthogonal Quality	Skewness	Average Grid Quality	Number of Nodes	Total Number of Grids
Scheme A	0.86	0.13	0.82	706,577	3,047,016
Scheme B	0.88	0.11	0.86	1,473,935	5,025,935
Scheme C	0.86	0.12	0.84	1,508,376	8,032,195

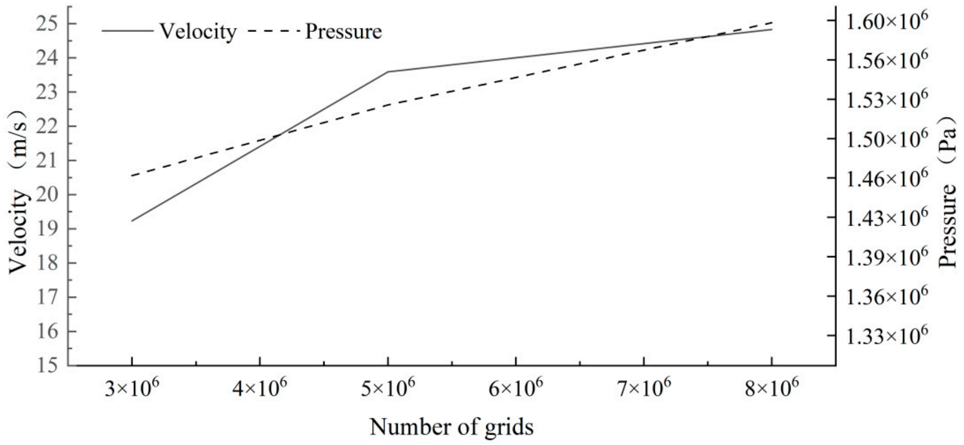

Figure 2. Grid independence test.

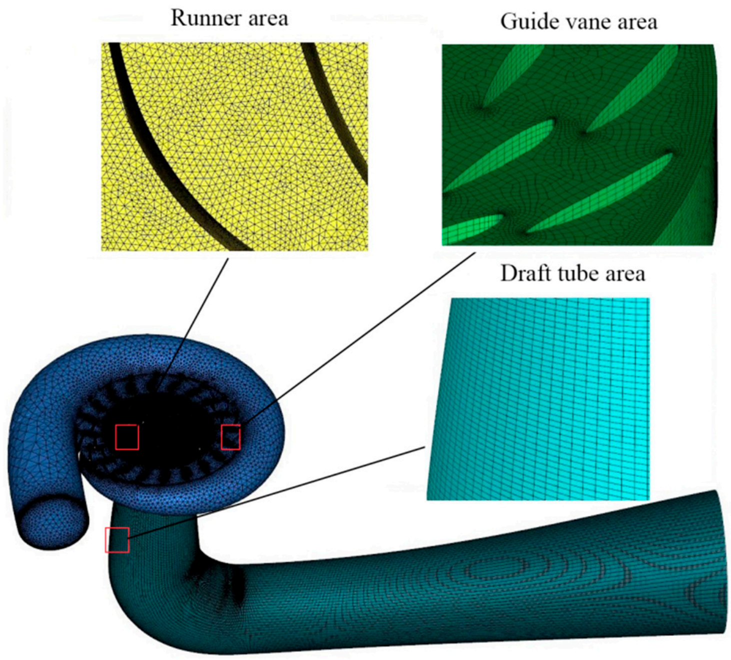

Figure 3. Grid division diagram.

2.3. Solution Settings

The runner in the 3D fluid domain model was rotating with the movement of the water, and it was set to the rotating domain. The spiral casing, stay vane, guide vane, and draft tube were set as stationary.

2.3.1. Governing Equations of Fluid Flow

The motion of fluids follows the mass conservation equation, momentum equation, and energy equation. The fluid in the turbine was incompressible, and the heat exchange capacity was so small that it can be ignored; the energy equation cannot be considered [26].

(1) Mass conservation equation:

$$\frac{\partial \rho}{\partial t} + \frac{\partial(\rho u_x)}{\partial x} + \frac{\partial(\rho u_y)}{\partial y} + \frac{\partial(\rho u_z)}{\partial z} = 0 \tag{1}$$

(2) Momentum equation:

$$\frac{\partial(\rho u_i)}{\partial t} + \frac{\partial(\rho u_i u_j)}{\partial x_j} = -\frac{\partial p}{\partial x_i} + \mu \frac{\partial^2 u_i}{\partial x_i x_j} \tag{2}$$

where P is the fluid pressure, ρ is the fluid density, μ is the fluid dynamic viscosity, and t is the time. u_i and u_j represent the components of velocity in the i and j directions, respectively. x_i and x_j represent the components of displacement in the i and j directions, respectively.

2.3.2. Boundary Conditions and Calculation Methods

(1) Boundary conditions

There was a dynamic and static interface between the guide vane and the runner and the runner and the draft tube. The multiple reference frame (MRF) model and sliding grid model were used to deal with the interface models [27]. In this paper, a multiple reference frame model was chosen to deal with the dynamic–static interface. A rotational speed was given in the rotation domain of the runner. The coordinate origin and direction of the runner rotation axis were set. The inlet and outlet walls were set to the interface. The inlet adopted the boundary condition of the velocity inlet, and the inlet velocity was determined based on the flow rate and spiral casing inlet area. The boundary condition of the pressure outlet was adopted for the outlet. The pressure at the outlet section of the draft tube was set to the outflow. The walls in the rotating domain of the runner were all set as moving walls. The solid walls all adopted nonslip boundary conditions. The near-wall surface adopted standard wall functions.

(2) Calculation methods

The internal flow field of a hydraulic turbine is complex. The traditional Reynolds Average Navier–Stokes (RANS) method was compared with the Large-Eddy Simulation method, and the latter can capture more turbulence details and obtain more comprehensive flow field information. The Smagorinsky–Lilly subgrid stress dynamic model in Large-Eddy Simulation was selected as the turbulence model. The finite volume method was used to establish discrete equations. A fully implicit format was used to discretize time. The second-order upwind scheme was adopted for convection term. The central difference scheme was used for the source and diffusion terms. The pressure-based solver and simple algorithm were used to solve the problem. The convergence criterion was set to 10^{-5}. The residual value reached 10^{-5}; it was considered as convergence [28,29].

2.4. Determination of Working Conditions

The opening of the guide vanes was adjusted to change the working conditions. This article selected the working conditions of 1%, 25%, 50%, 75%, and 100% of the opening of the guide vanes to conduct three-dimensional transient simulation. Flow characteristics under different working conditions were analyzed. The calculation parameters for each working condition are shown in Table 3.

Table 3. Calculation Parameters of Operating Points.

Operation point	100%Pn	75%Pn	50%Pn	25%Pn	1%Pn
Guide vane opening (mm)	19.02	14.64	12.24	9.78	4.55
Inlet velocity (m/s)	19.15	15.07	12.02	9.75	3.53

3. Results

3.1. The Pressure Distribution of the Guide Vane

The pressure distribution of the guide vane is shown in Figure 4. The distribution of pressure in the circumferential direction was basically symmetrical. The pressure was mainly concentrated in the stay vane area and the outer area of the guide vane. The water flow from the spiral casing into the guide vane caused head loss, which will impact the guide vane and cause the pressure to decrease radially. The flow velocity increased uniformly along the radial direction as the flow channel narrowed. The angle of attack between the guide vane and the water flow was very small, and the head loss was very small. The pressure distribution in the stay vane area was basically consistent. The guide vane opening decreased, and the pressure magnitude in the stay vane area decreased. The maximum pressure value in the stay vane area was 1.26×10^7 Pa at 100% working condition. The maximum pressure value in the stay vane area was 1.20×10^7 Pa at 75% working condition. The maximum pressure value in the stay vane area was 9.94×10^6 Pa at 50% working condition. The maximum pressure value in the stay vane area was 7.83×10^6 Pa at 25% working condition. The lowest pressure value in the stay vane area was only 4.3×10^6 Pa at 1% working condition. The above pressure distribution conformed to the theoretical design, and it proved that the placement angle of the guide vanes was reasonable. It reduced head loss and improved the performance of the hydraulic turbine.

The water flow from the stay vane impacted the guide vane at a certain angle of attack, which produced a small detachment near the guide vanes. The placement angle of the guide vane was optimal, and the impact strength of the water flow on the guide vane was minimal at 100% working condition. It produced a smaller head loss and a larger wake area. The working conditions were further reduced, the opening of the guide vane decreased, and the impact between water flow and the guide vane increased at 75% and 50% working conditions. It produced a larger head loss and a smaller wake area. The pressure in the guide vane area was less than 1×10^7 Pa. The wake area further decreased, and the pressure in the guide vane area was about 4×10^6 Pa at 25% working condition. The guide vanes hindered most water flow under 1% working condition. The pressure was concentrated at the head of the guide vane, and there was no obvious wake area. The pressure distribution measured inside the guide vane was basically consistent, and the pressure in the guide vane area was about 2×10^6 Pa, which was much lower than the pressure on the outer side of the guide vane.

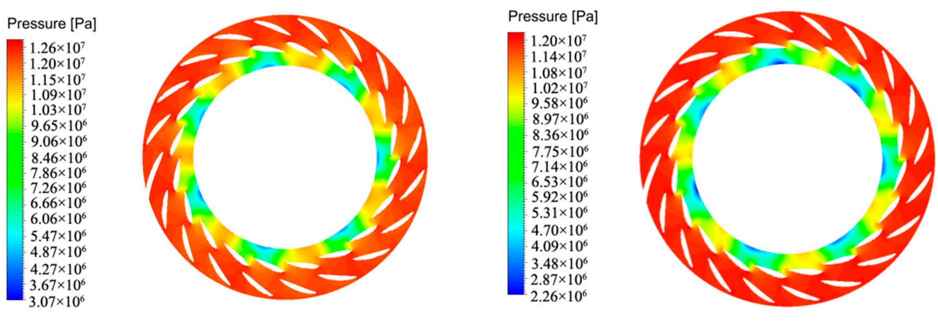

(**a**) (**b**)

Figure 4. *Cont.*

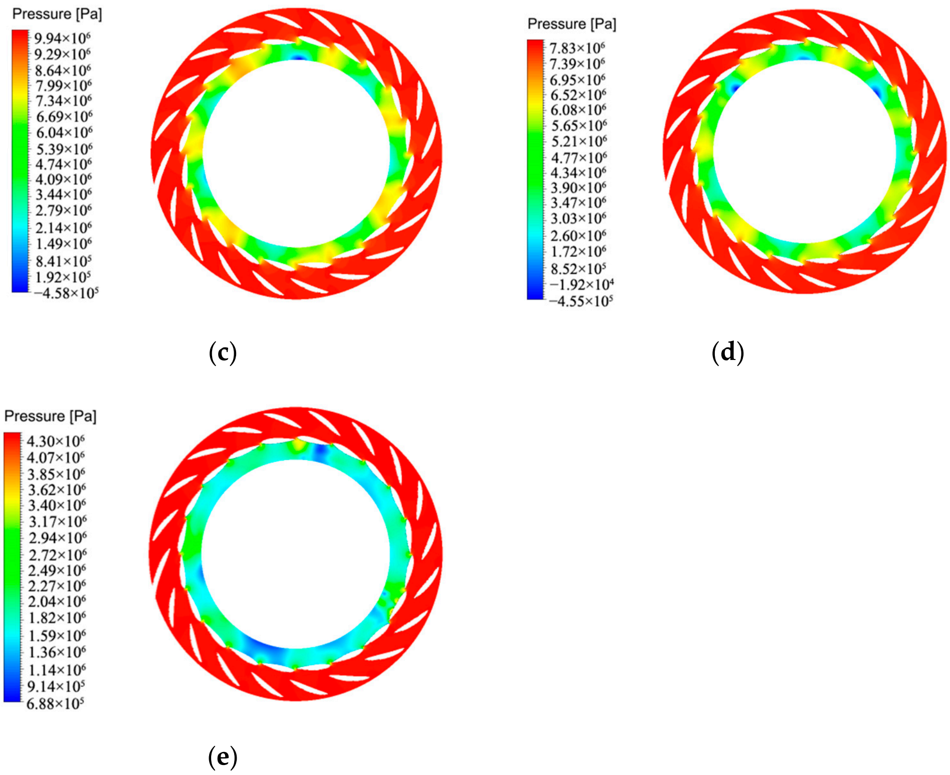

Figure 4. Pressure cloud map of guide vane center profile: (**a**) Pressure cloud map of guide vane center profile at 100%Pn. (**b**) Pressure cloud map of guide vane center profile at 75%Pn. (**c**) Pressure cloud map of guide vane center profile at 50%Pn. (**d**) Pressure cloud map of guide vane center profile at 25%Pn. (**e**) Pressure cloud map of guide vane center profile at 1%Pn.

Overall, the pressure distribution in the stay and guide vanes had good symmetry, and the pressure decreased radially. The placement angle of the guide vanes was reasonable. It provided good inflow conditions and improved turbine performance.

3.2. Flow Distribution of the Runner

(1) Pressure distribution in the center profile of the runner

The pressure distribution in the center profile of the runner is shown in Figure 5. The pressure distribution of each working condition was similar from an overall point of view. The pressure distribution of the runner was symmetrical in structure in the circumferential direction. There was local high pressure at the head of the blade pressure surface, and there was part of the negative pressure area at the suction surface of the blade. The pressure of the runner blade from the inlet side to the outlet side showed a decreasing trend, and the upper crown to the lower ring also showed a decreasing trend. The pressure difference between the front and back of the runner blades had more water flow into the blade channel.

Water flowed out of the guide vanes and impacted the runner blades at a certain angle of attack. This indicated the presence of a high-pressure region at the tail of the pressure surface of the runner blade, and a partial negative pressure area was generated at the water inlet edge of the blade suction surface. The high-pressure area of the blade pressure surface and the negative pressure area of the suction surface were the largest at 100% working condition. The negative pressure area accounted for almost two-thirds of the blade channel area. The pressure in the pressure surface area was 1.24×10^7 Pa, and the pressure in the suction surface area was -3×10^6 Pa. There was a pressure difference between the front and back sides of the blade, and the water was sucked into the runner blade channel. Part of the water flowed along the blade channel into the draft tube. Another part of the water flow impacted adjacent blades at a certain angle, and it caused detachment under the action of uneven protrusions on the blade surface. This can easily generate blade channel vortices.

Sun et al. [18] reached a similar conclusions through experimental verification. The working conditions further decreased, and the high-pressure area of the pressure surface and the negative pressure area of the suction surface gradually decreased. The distribution pattern of the runner area at 75% working condition was similar to that at 100% working condition, and it only slightly reduced the high-pressure area of the pressure surface and the negative pressure area of the suction surface. The high-pressure area of the pressure surface and the negative pressure area of the suction surface further reduced at 50% working condition. The high-pressure area on the pressure surface and the negative pressure area on the suction surface were almost nonexistent at 25% working condition. The pressure on both sides of most areas of the runner blades was basically the same, and the pressure was about 9.7×10^5 Pa. Local pressure difference only existed at the blade head.

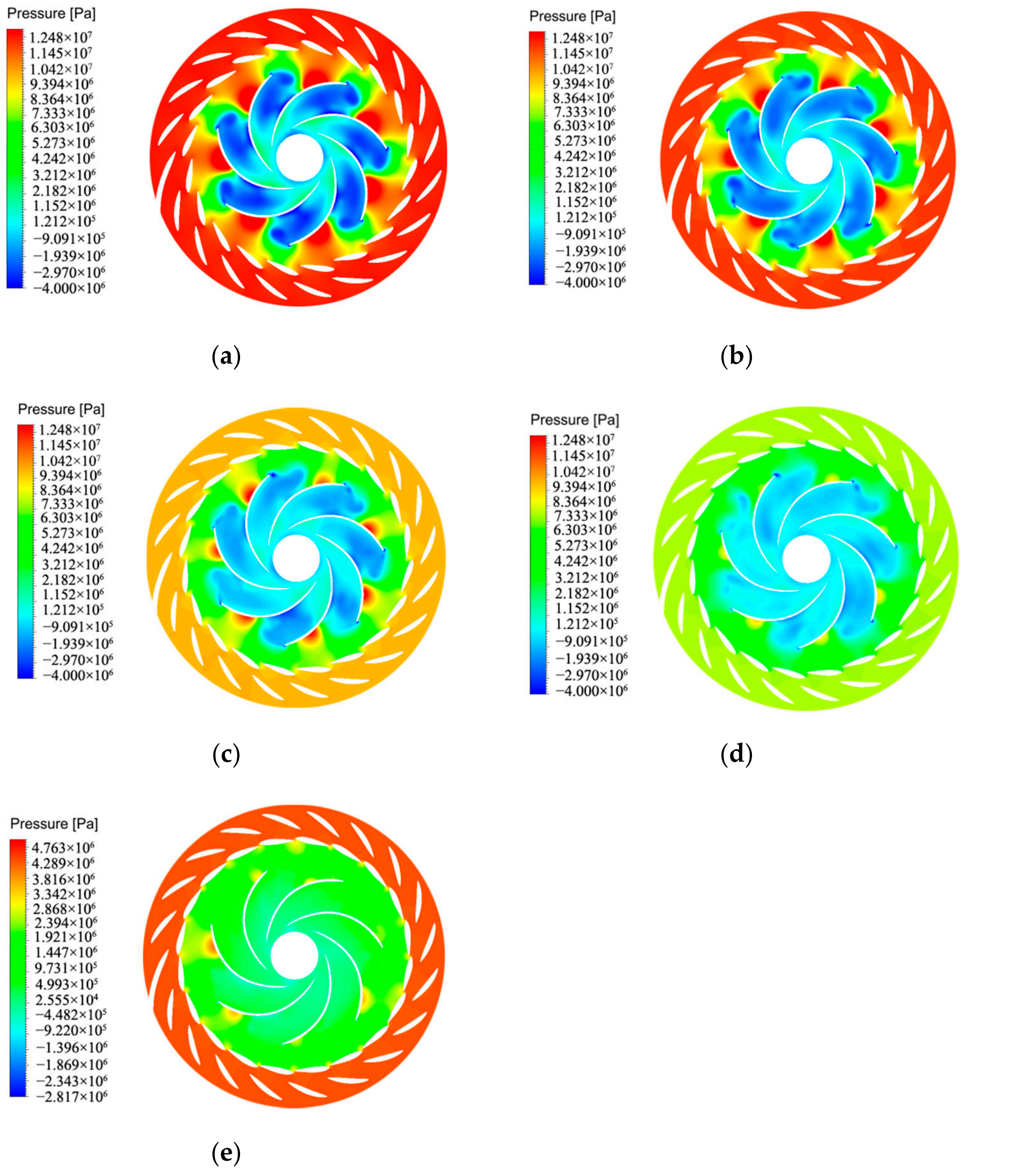

Figure 5. Pressure cloud map of the center section of the runner: (**a**) Pressure cloud map of the center section of the runner at 100%Pn. (**b**) Pressure cloud map of the center section of the runner at 75%Pn. (**c**) Pressure cloud map of the center section of the runner at 50%Pn. (**d**) Pressure cloud map of the center section of the runner at 25%Pn. (**e**) Pressure cloud map of the center section of the runner at 1%Pn.

Overall, the pressure distribution in the runner area was symmetrical. The pressure difference between the front and back surfaces of the blades caused the runner blades to rotate, and it ensured the normal operation of the hydraulic turbine. Compared with the existing hydraulic turbines, the pressure distribution of the runner blades was more reasonable. However, the impact of water flow on the blades caused flow separation and detachment, and it generated vortex structures in the blade channel. This reduced the performance of the turbine and decreased its longevity. Appropriate measures should be sought to suppress vortex structures.

(2) Streamline distribution at different blade heights and flow surfaces within the runner

The flow characteristics under 50% working conditions were obvious and had good representativeness. The streamline diagrams of the 10% blade high-flow surface, 50% blade high-flow surface, and 90% blade high-flow surface of the runner were extracted under 50% working conditions. The streamline distributions of different blade height flow surfaces at the same position were compared. Significantly different areas in the streamline distribution were selected for amplification (Figure 6). The flow velocity at the inlet position of the pressure surface of the runner blade was the maximum. The head loss caused by the impact of the blades made the water flow into the blade channel at a relatively small velocity. The flow velocity in the vortex structure area at the center of the blade channel was minimized under the action of the channel vortex. The pressure difference between the front and back sides of the runner blades had more water flow into the blade channel, which resulted in varying degrees of vortex regions on the runner blades starting from the head. The vortex structures at the high-flow surfaces of each blade were similar in shape and approximate elliptical vortex structures. The streamline distribution on each flow surface exhibited a symmetrical structure in the circumferential direction, and there was a severe flow detachment at the blade inlet. The vortex structure at the head of the blade channel was obvious near the upper crown. The lateral flow at the head of the blade channel was obvious near the lower ring. This indicated that the water flow was severely impacted at the blade inlet and caused significant head loss.

It can be seen in Figure 6a that a distinct channel vortex was generated in the head area of the blade channel. The opening of the guide vane was relatively small, and the water flow impacted the runner blades at a relatively large angle of attack. Flow separation occurred in the water flow, and it formed two parts of the water flow. A part of the water flowed along one side of the blade suction surface towards the tail of the blade channel. Another part of the water flow broke free from the constraints of the blades under the action of uneven protrusions on the surface of the blades. This indicated that the detachment phenomenon had occurred, and vortex structures were created in the blade channel. The effect of channel vortices consumed most of the kinetic energy of the water flow, a low-speed region was generated in the channel vortex region, and some water flow velocities were even 0 m/s. It can be seen in Figure 6b that the vortex structure increased, the vortex area increased, and the water flowed from the head of the blade channel to the tail. The low-speed area in the middle of the blade channel also increased under the action of the blade channel vortex. The vortex structure compressed water flow, water flowed laterally at both the head and tail of the blade channel, and it generated greater head loss. It can be seen in Figure 6c that there was no obvious vortex structure at the head of the blade channel, and it was mainly concentrated in the tail area of the blade channel. The transverse flow area was distributed across the entire blade channel, and it caused severe head loss. The efficiency of the water turbine decreased.

Overall, water flowed into the blade channel and impacted the blade at a certain angle of attack, which led to the appearance of vortex structures in the flow channel. The vortex structure moved from the head to the tail, the vortex structure area gradually increased, and the transverse flow area increased from the upper crown of the runner to the lower ring. The water flow in the runner channel carried a large circumferential circulation, and the water flowed into the draft tube in the form of vortex structure. The flows in the draft tube intertwined with each other, which formed an eccentric vortex rope in the draft tube, and it led to the vibration of the hydraulic turbine. This reduced turbine performance and decreased turbine longevity.

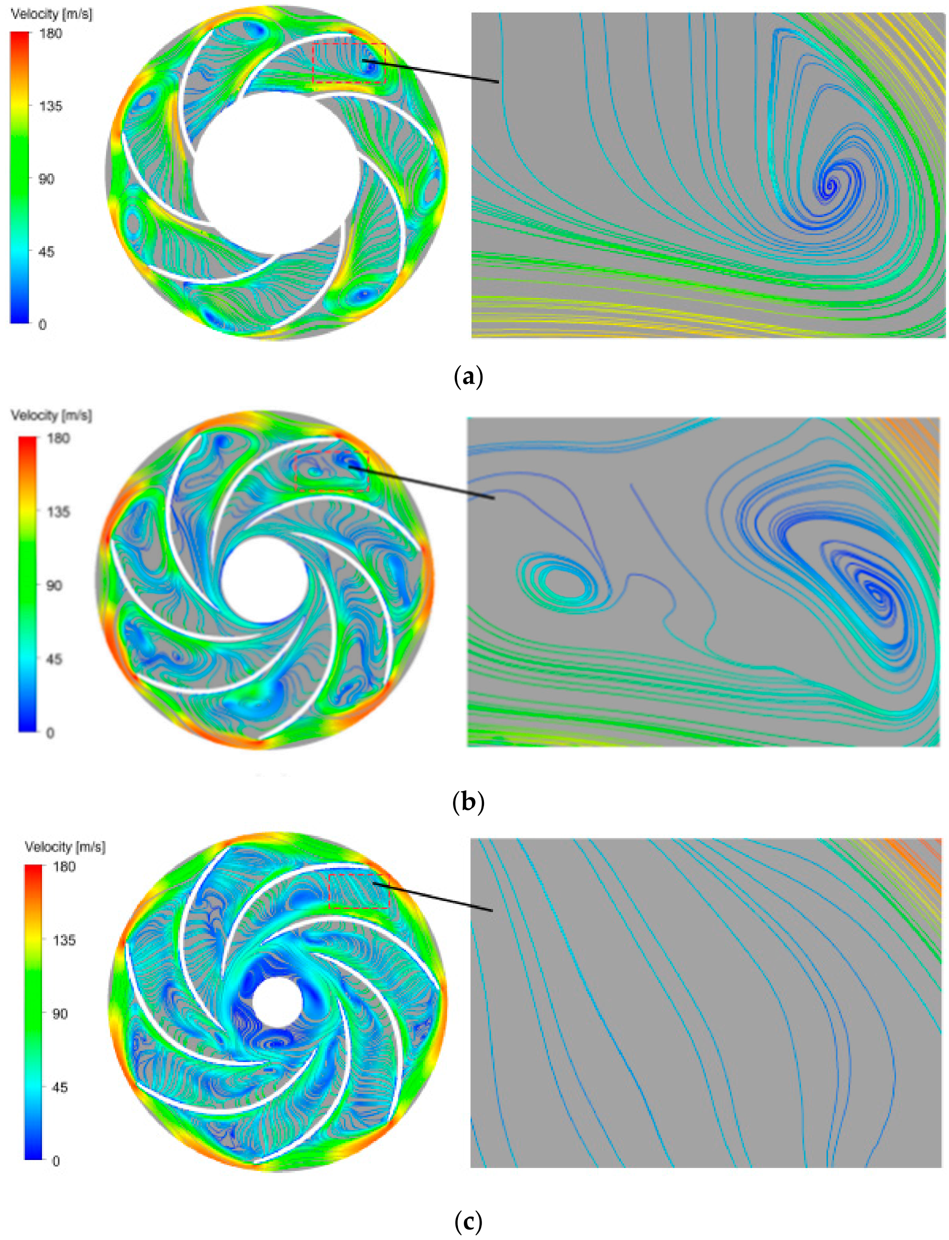

Figure 6. Streamline cloud map of the high-flow surface of the blades: (**a**) Streamline cloud map of 90% blade height flow surface. (**b**) Streamline cloud map of 50% blade height flow surface. (**c**) streamline cloud map of 10% blade height flow surface.

(3) Distribution of vortex cores in the runner

The vortex core diagram is shown in Figure 7. The vortex structures under different working conditions were symmetrically distributed in the circumferential direction. The flow pattern in the guide vane area was stable. Only small-scale vortex structures were generated at the head of the guide vane. Vortex structures of different sizes and shapes appeared between the runner blade flow channels. The pressure difference between the pressure surface and suction surface caused the water flow into the middle of the blade, and the water flow formed a flow separation at the leading edge of the blade and flowed into the blade channel along the front and back sides of the blade. The detachment and flow separation were generated under the action of uneven protrusions on the surface of the blade, which led to the formation of vortex structures in the middle of the blade channel, such as pipeline vortices between the blades.

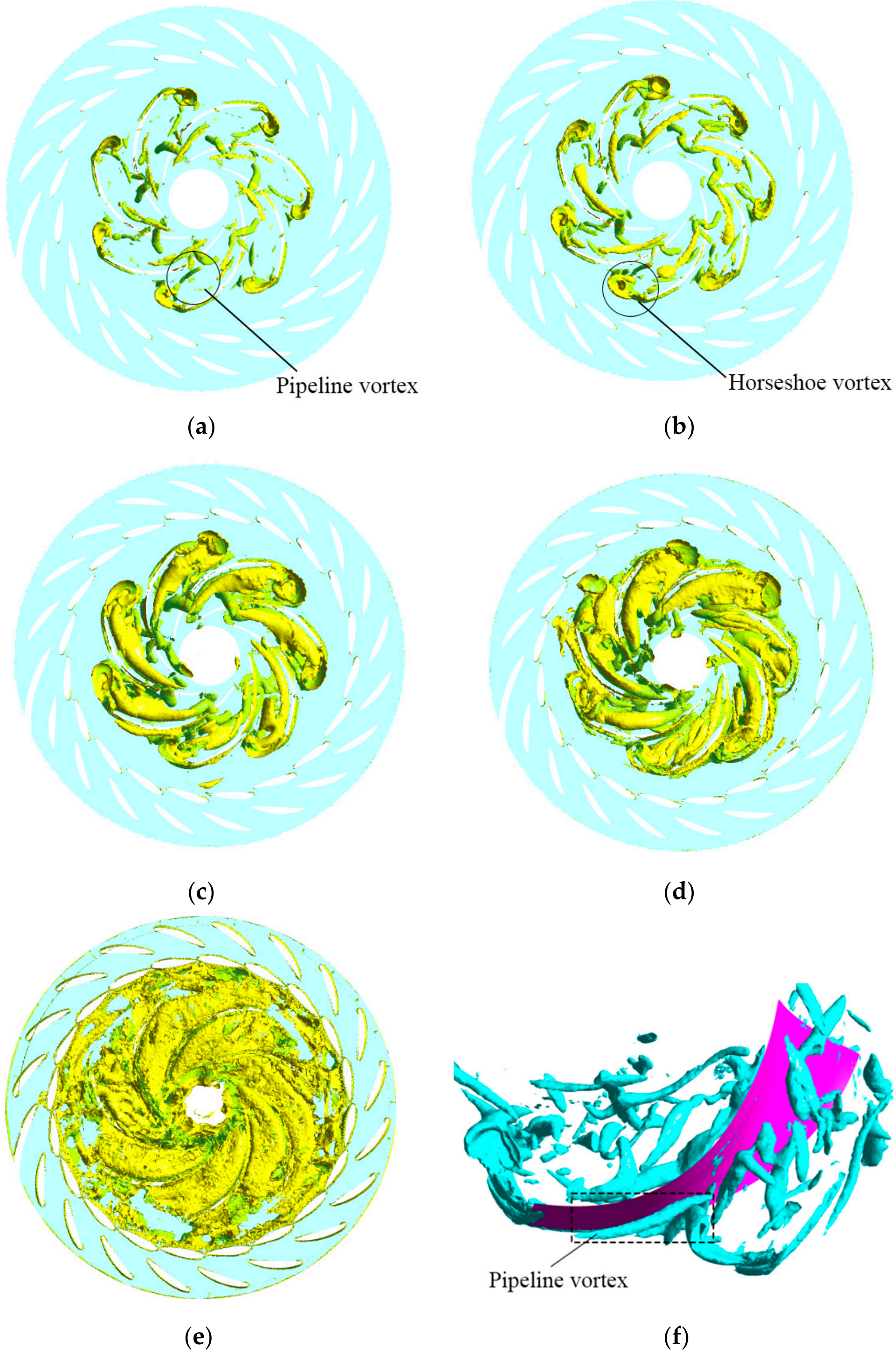

Figure 7. Vortex core in the runner area: (**a**) Vortex core diagram of runner area at 100%Pn. (**b**) Vortex core diagram of runner area at 75%Pn. (**c**) Vortex core diagram of runner area at 50%Pn. (**d**) Vortex core diagram of runner area at 25%Pn. (**e**) Vortex core diagram of runner area at 1%Pn. (**f**) Vortex structure near blades at 100%Pn.

The placement angle of the guide vane was the best at 100% working condition. The direction of the inlet water flow streamline was consistent with the tangential direction of the inlet runner blade. In theory, there was no impact of inlet water flow on the blades, and due to the rotation of the runner blades affecting the movement of water in the guide vane area, there was a small angle of attack and small-scale vortex structures. In reference [30], the same conclusion was reached after experimental verification. It was shown that there was an oval horseshoe vortex at the head of the blade channel and a long pipe vortex between the blade channels.

The flow rate decreased as the working conditions decreased. The blades were impacted by a larger angle of water flow, which led to a more obvious flow separation phenomenon. The more vortex structures were generated between blade channels, the more pipe vortex and horseshoe vortex structures existed between blade channels. The opening of the guide vane was very small at 1% working condition. More vortex structures can also be seen in the guide vane area, which almost covered the entire runner blade channel area. This seriously affected the normal operation of the water turbine and reduced its longevity.

(4) Pressure distribution on the surface of runner blades

The distribution law of blade surface pressure was studied at 50% working conditions. The pressure of the runner blade was symmetrically distributed in the circumferential direction. A blade was picked at random, and horizontal and vertical lines were drawn along the pressure and suction surfaces of the rotor blade. The pressure distribution on a straight line was measured, and the straight-line distribution is shown in Figure 8.

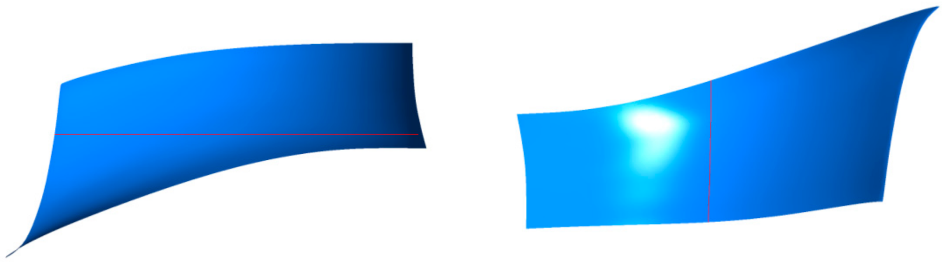

(**a**) (**b**)

Figure 8. Line distribution: (**a**) horizontal line distribution and (**b**) vertical line distribution.

As shown in Figure 9a, the highest pressure position was located at the blade head, which was approximately 1.5×10^7 Pa. The suction surface pressure of the blade was lower than the pressure surface in most areas. It was in a negative pressure state, and the fluctuation was not very obvious. There were only some areas where the pressure was higher than the pressure surface at the water outlet edge and the middle position of the blade. The pressure difference between the pressure and suction surfaces of the runner blades gradually increased from the outlet to the inlet. The cavitation phenomenon at the head of the runner blade was stronger than that at the tail of the blade. This is because the water flow from the guide vane impacted the pressure surface of the runner blade at a large angle of attack, and it led to local high pressure at the head of the blade pressure surface.

As shown in Figure 9b, the pressure distribution pattern of the pressure surface and suction surface in the vertical direction was basically the same. From the top crown to the bottom ring, the pressure first increased, then decreased, and then increased again. The pressure on the front of the runner blades was less than the pressure on the back. The pressure on the front was negative pressure. This confirmed the conclusion drawn from the pressure distribution on the horizontal straight line above. There were some areas in the middle of the blade where the front pressure was lower than the back pressure.

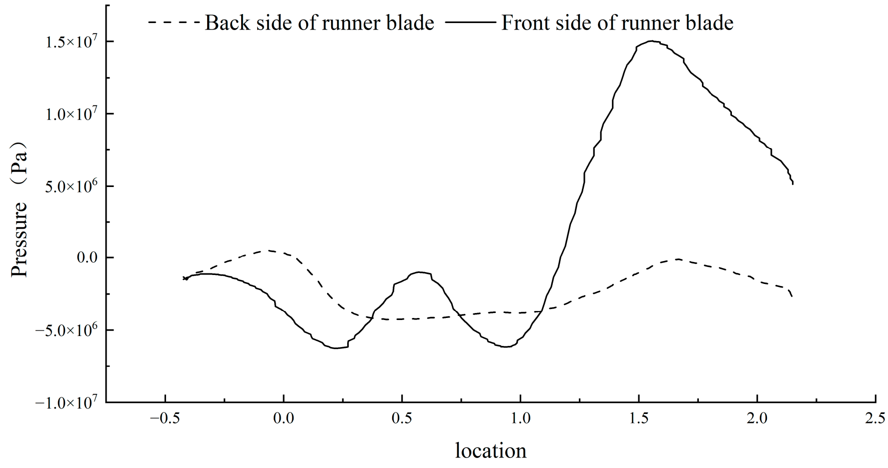

(**a**)

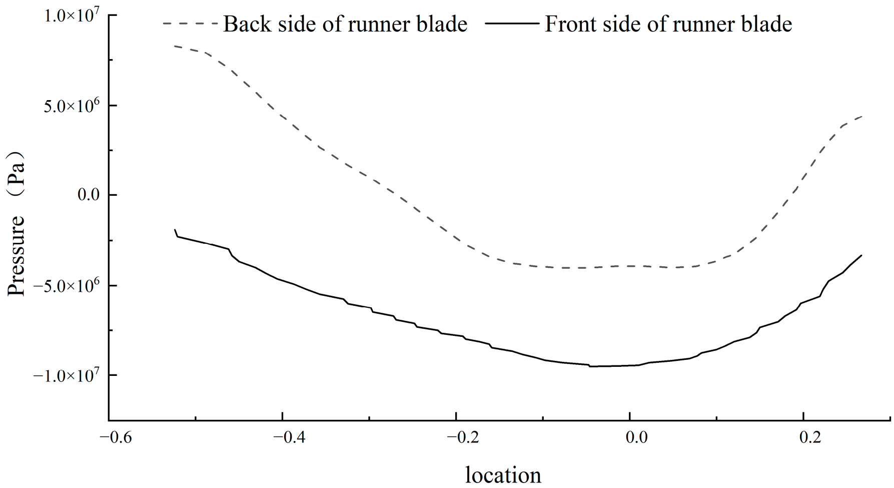

(**b**)

Figure 9. Pressure distribution diagram of the front and back of the runner blade: (**a**) horizontal linear pressure distribution diagram and (**b**) vertical linear pressure distribution diagram.

3.3. The Flow Distribution in Draft Tube

(1) Velocity distribution of draft tube

The flow velocity diagram of the draft tube under different guide vane openings is shown in Figure 10. The flow from the runner impacted the draft tube wall with a large circumferential velocity. The velocity on the side wall of draft tube was greater than that in the center of draft tube. The maximum flow velocity area on the sidewall accounted for the largest proportion at 100% working condition. It extended from the straight cone section sidewall to the curved elbow section sidewall, and the maximum flow velocity was 51 m/s. The decrease in inlet flow rate led a gradual decrease in the flow velocity on the side wall of the straight cone section of the draft tube as the opening decreased. The maximum flow velocity area was mainly concentrated on the edge wall of the straight cone section at 50% working condition. There was almost no maximum flow velocity region on the side wall of the elbow section. The maximum flow velocity region only existed on the inlet wall of the draft tube as the opening further decreased.

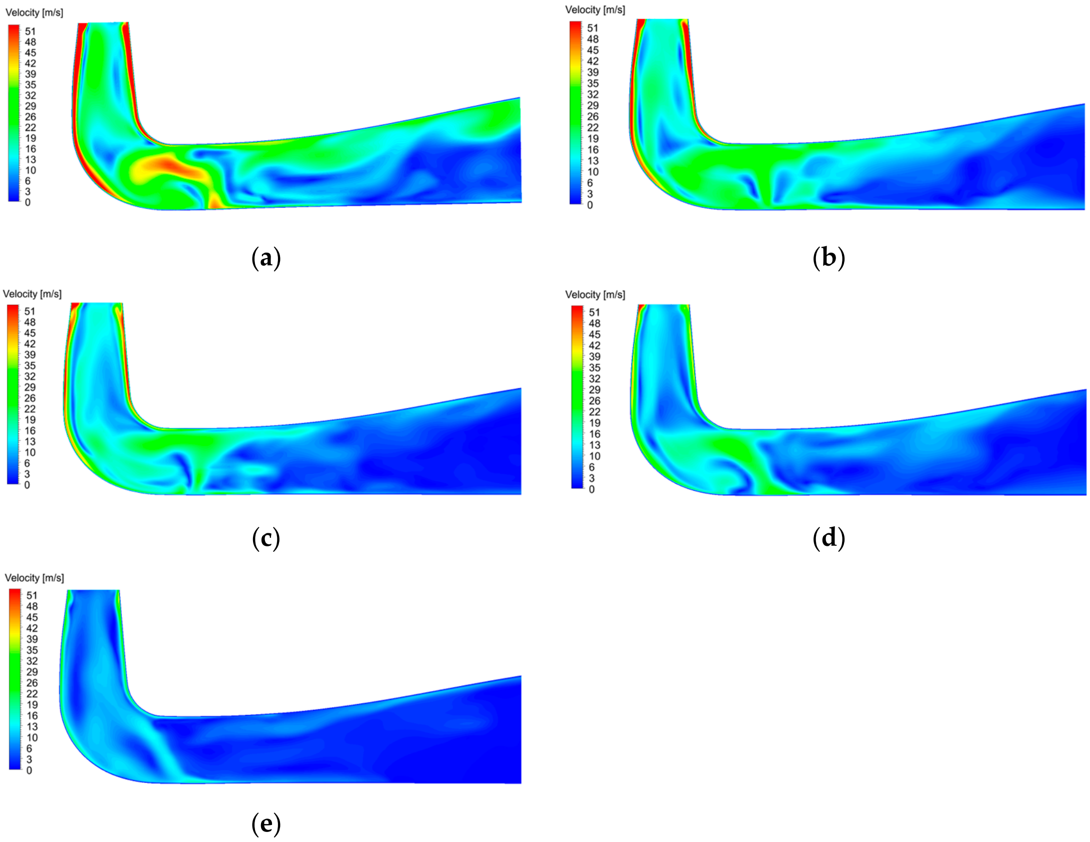

Figure 10. Flow rate diagram of draft tube: (**a**) Velocity diagram of draft tube at 100%Pn. (**b**) Velocity diagram of draft tube at 75%Pn. (**c**) Velocity diagram of draft tube at 50%Pn. (**d**) Velocity diagram of draft tube at 25%Pn. (**e**) Velocity diagram of draft tube at 1%Pn.

The side wall of the draft tube changed at a large angle at the elbow, and the water flowed out of the straight cone section and impacted the elbow of draft tube with a large impact angle. The flow at the elbow of draft tube was disordered to varying degrees under different working conditions. The flow velocity in the central area of the draft tube was maximal at 100% working condition. The chaos caused by the impact in the elbow section was the greatest, and there was a significant high-flow-velocity area in the center area of the elbow section. The working conditions decreased, the flow velocity in the elbow section decreased at 75% working condition, and the flow velocity was about 30 m/s. The flow velocity distribution in the elbow section was uniform as the working conditions decreased, and chaos significantly decreased here at 50% working condition. The flow velocity in the elbow section was minimal at 1% working condition, and the flow velocity was 10 m/s.

The chaotic water flow was transmitted to the downstream diffusion section, which had a certain impact on the flow pattern of the downstream water flow, and the opening decreased, the effect of which became more inapparent. There were two parts in the diffusion section at 100% working condition. The flow velocity in the upper region was significantly higher than that in the lower region. A large flow velocity difference indicated a significant pressure difference, and it led to cavitation in some areas. This caused water to flow back from the outlet of the draft tube to the draft tube. The vortex structures were prone to appear in the diffusion zone under the action of two parts of water flow. The low-speed area parts in the diffusion section increased, and they were concentrated at the outlet at 75% working condition. This reduced the backflow phenomenon. The low-speed area of the diffusion section increased as the working conditions decreased. The water flow velocity in the entire draft tube area was very low at 1% working condition.

The role of the draft tube was mainly reflected in the diffusion section. The water flowed out of the runner and carried a large amount of kinetic energy. Most of the energy was consumed when the water flowed through the diffusion section of the draft tube. The water was allowed to flow out of the turbine at a smaller velocity. However, cavitation occurred in some working conditions due to the flow velocity difference in the diffusion section. This caused external water flow to be sucked into the draft tube, and it caused two parts of water to impact each other, forming a vortex structure. The vortex structure can cause vibration and noise in the water turbine. It will reduce the performance of the water turbine and even reduce its longevity. It was necessary to find appropriate measures to reduce the flow velocity in the diffusion zone.

(2) The streamline distribution of draft tube

The streamline diagram of the draft tube is shown in Figure 11. The streamline distribution was different under different working conditions. The vortex structure appeared in the straight cone section, which was caused by the low flow velocity in the center of the draft tube, and it caused the water flow to converge inward. The flow pattern in the elbow section was relatively stable, and there was no obvious vortex structure. In the diffusion section, the upper water flow streamline was evenly distributed, and vortex structures of varying sizes appeared in the lower part. The reason is due to the flow velocity in the diffusion section being nonuniform, which led to backflow in the draft tube. The flow left above the draft tube collided with the flow returning from the draft tube outlet at the lower part of the diffuser. This caused flow separation and formed a vortex structure. The vortex structure at 1% working condition was the most obvious.

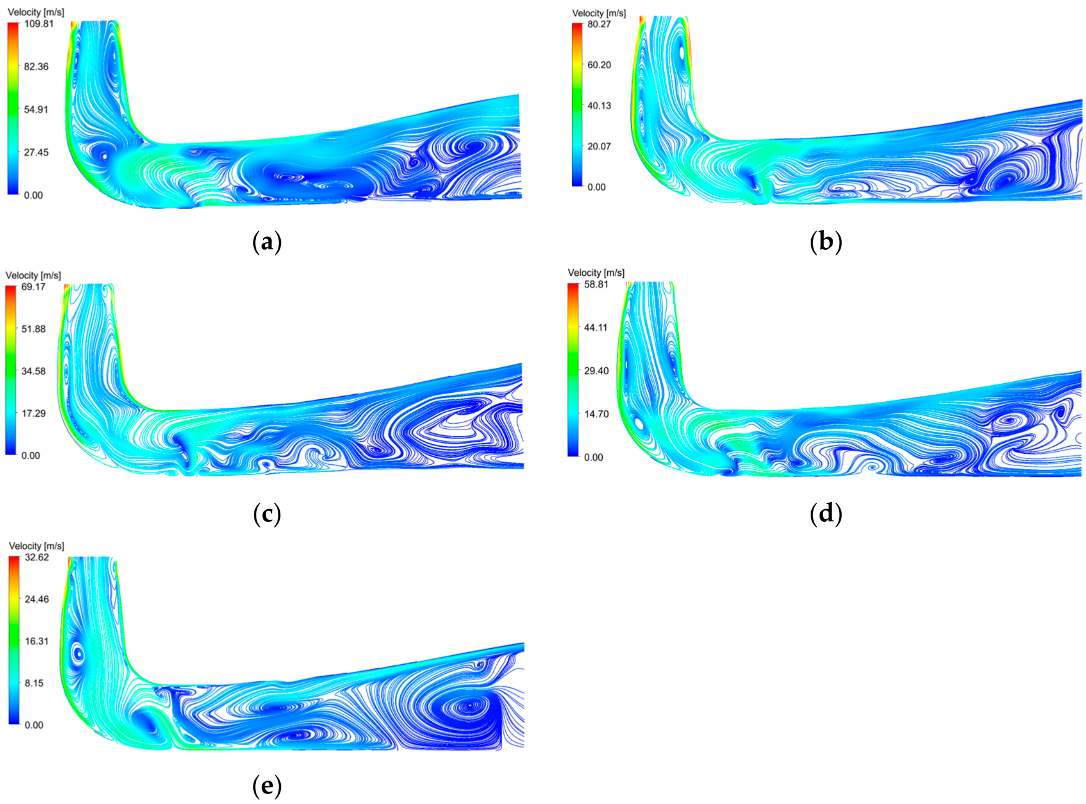

Figure 11. Draft tube flowline diagram: (**a**) Draft tube flowline diagram at 100%Pn. (**b**) Draft tube flowline diagram at 75%Pn. (**c**) Draft tube flowline diagram at 50%Pn. (**d**) Draft tube flowline diagram at 25%Pn. (**e**) Draft tube flowline diagram at 1%Pn.

(3) The pressure and velocity distribution of the draft tube outlet section

The maximum velocity and pressure distribution diagram at the opening section of the draft tube under different openings is presented in Figure 12. The pattern of change was the same. The working conditions decreased, and the opening of the guide vanes decreased accordingly. The inlet flow rate decreased, and the flow rate decreased accordingly. The minimum flow rate was at 1% working condition, which was 8 m/s. The smaller the working condition, the smaller the draft tube outlet pressure. The maximum pressure was concentrated near the draft tube wall.

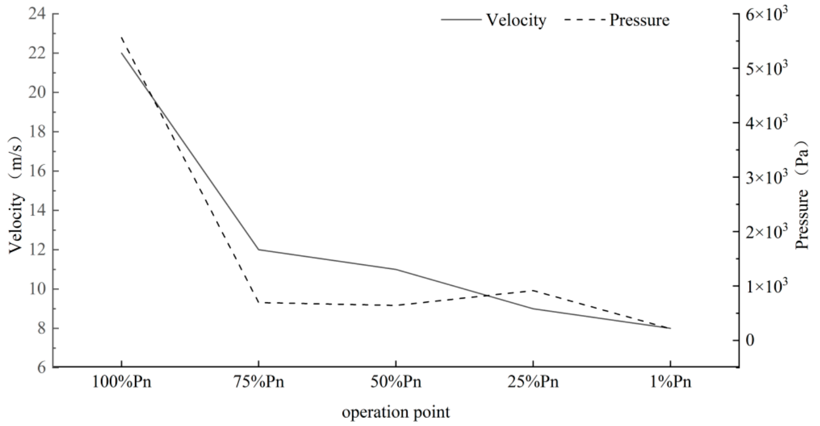

Figure 12. Maximum velocity and pressure at the outlet section of the draft tube under different working conditions.

4. Conclusions

In this paper, a three-dimensional unsteady turbulent numerical simulation of a Francis turbine was carried out based on the Large-Eddy Simulation. The flow characteristics of each component under different working conditions were analyzed, and the hydraulic performance of each part was evaluated. The factors that affected the stability of hydraulic turbines were identified, and their formation mechanisms and evolution laws were explored.

(1) The pressure distribution of each working condition was similar from an overall point of view. The pressure difference between the front and back surfaces of the blades caused the runner blades to rotate, and it ensured the normal operation of the hydraulic turbine. However, the hydraulic performance was poor in the runner area, and there were flow separation and detachment phenomena in the flow field. The cavitation phenomenon occurred inside the runner, which generated channel vortex. The vortex structures of different scales were distributed between runner blades, and a horseshoe vortex and pipe vortex were captured under some working conditions. The channel vortex promoted the lateral flow of water and had a significant impact on the stability of the hydraulic turbine. The water flowed into the draft tube in the form of a vortex structure. This reduced turbine performance and decreased turbine longevity.

(2) The diffusion section of the draft tube can dissipate most of the kinetic energy of the water flow in the draft tube area, and it had a good energy dissipation effect. However, the large pressure difference between the upper and lower regions of the diffusion section generated a backflow phenomenon. Cavitation occurred in the draft tube. It created vortex structures in the draft tube, and the stability of the hydraulic turbine was greatly affected. The vortex structure can cause vibration and noise in the water turbine. This reduces the performance and longevity of hydraulic turbines. It is necessary to find appropriate measures to reduce the flow velocity in the diffusion zone in the future.

Author Contributions: Q.Y. and X.H. contributed to the conception, guidance, and revising of the manuscript. The software analysis was conducted by C.L. The manuscript was written by Q.C. and T.X. All authors have read and agreed to the published version of the manuscript.

Funding: This work was supported by the Basic Scientific Research Fund of Heilongjiang Provincial Universities: (2021-KYYWF-0050).

Data Availability Statement: The data that support the finding of this study are available from the corresponding author upon reasonable request.

Acknowledgments: The authors acknowledge the co-operation and support of School of Hydraulic and Electric Power, Heilongjiang University, Harbin 150080, China for this research.

Conflicts of Interest: The authors declare no conflict of interest.

References

1. Li, Y.; Ji, P. The status quo analysis and policy suggestions on promoting China's hydropower development. *Renew. Sustain. Energy Rev.* **2015**, *51*, 1071–1079. [CrossRef]
2. Shen, J.; Cheng, C.; Shen, Q.; Lu, J.; Zhang, J. Overview of China's hydropower absorption: Evolution, problems, and suggested solutions. *IET Renew. Power Gener.* **2019**, *13*, 2491–2501. [CrossRef]
3. Lin, T.; Zhang, J.; Li, J.; Li, X.; Zhu, Z. Pressure Fluctuation–Vorticity Interaction in the Volute of Centrifugal Pump as Hydraulic Turbines (PATs). *Processes* **2022**, *10*, 2241. [CrossRef]
4. Hu, X.; Zhang, L. Vortex Cascade Features of Turbulent Flow in Hydro-Turbine Blade Passage with Complex Geometry. *Water* **2018**, *10*, 1859. [CrossRef]
5. Wang, S.; Zhang, L.; Yin, G.; Guan, C. Research on Unsteady Hydraulic Features of a Francis Turbine and a Novel Method for Identifying Pressure Pulsation Transmission Path. *Water* **2019**, *11*, 1216. [CrossRef]
6. Tran, C.; Pham, D. Application of Liutex and Entropy Production to Analyze the Influence of Vortex Rope in the Francis-99 Turbine Draft Tube. *Tech. Gaz.* **2022**, *29*, 1177–1183.
7. Li, P.; Tao, R.; Yang, S.; Zhu, D.; Xiao, R. Temporal and Spatial Analysis on the Fractal Characteristics of the Helical Vortex Rope. *Fractal Fract.* **2022**, *6*, 477. [CrossRef]
8. Goyal, R.; Trivedi, C.; Gandhi, B. Numerical Simulation and Validation of a High Head Model Francis Turbine at Part Load Operating Condition. *J. Inst. Eng. Ser. C* **2018**, *99*, 557–570. [CrossRef]
9. Yu, A.; Wang, Y.; Zhou, D. Vortex Evolution and Energy Production in the Blade Channel of a Francis Turbine Operating at Deep Part Load Conditions. *J. Appl. Fluid Mech.* **2021**, *14*, 1669–1678.
10. Zhou, L.; Liu, M.; Wang, Z.; Liu, D.; Zhao, Y. Numerical simulation of the blade channel vortices in a Francis turbine runner. *Eng. Comput.* **2017**, *34*, 364–376. [CrossRef]
11. Su, W.; Li, X.; Li, F.; Wei, X.; Han, W.; Liu, S. Experimental Investigation on the Characteristics of Hydrodynamic Stabilities in Francis Hydroturbine Models. *Adv. Mech. Eng.* **2014**, *6*, 486821. [CrossRef]
12. Yan, X.; Kan, K.; Zheng, Y.; Chen, H. Entropy Production Evaluation within a Prototype Pump-Turbine Operated in Pump Mode for a Wide Range of Flow Conditions. *Processes* **2022**, *10*, 2058. [CrossRef]
13. Cheng, H.; Zhou, L.; Liang, Q.; Guan, Z.; Liu, D.; Wang, Z.; Kang, W. The investigation of runner blade channel vortices in two different Francis turbine models. *Renew. Energy* **2020**, *156*, 201–212. [CrossRef]
14. Liu, D.; Liu, X.; Zhao, Y. Experimental Investigation of Inter-Blade Vortices in a Model Francis Turbine. *Chin. J. Mech. Eng.* **2017**, *30*, 854–865. [CrossRef]
15. Liu, M.; Zhou, L.; Wang, Z.; Liu, D.; Zhao, Y. Investigation of Channel Vortices in Francis Turbines. *IOP Conf. Ser. Earth Environ. Sci.* **2016**, *49*, 082003. [CrossRef]
16. Zhang, R.; Mao, F.; Wu, J.; Chen, S.; Wu, Y.; Liu, S. Characteristics and Control of the Draft-Tube Flow in Part-Load Francis Turbine. *J. Fluids Eng.* **2009**, *131*, 539–544. [CrossRef]
17. Tran, C.; Ji, B.; Long, X. Simulation and Analysis of Cavitating Flow in the Draft Tube of the Francis Turbine with Splitter Blades at Off-Design Condition. *Tech. Gaz.* **2019**, *26*, 1650–1657.
18. Sun, L.; Guo, P.; Wu, L. Numerical investigation of alleviation of undesirable effect of inter-blade vortex with air admission for a low-head Francis turbine. *J. Hydrodyn.* **2020**, *32*, 1151–1164. [CrossRef]
19. Zhou, X.; Wu, H.; Shi, C. Numerical and experimental investigation of the effect of baffles on flow instabilities in a Francis turbine draft tube under partial load conditions. *Adv. Mech. Eng.* **2019**, *11*, 1687814018824468. [CrossRef]
20. Zhou, X.; Shi, C.; Miyagawa, K.; Wu, H. Effect of modified draft tube with inclined conical diffuser on flow instabilities in Francis turbine. *Renew. Energy* **2021**, *172*, 606–617. [CrossRef]
21. Guo, T.; Zhang, J.; Luo, Z. Analysis of Channel Vortex and Cavitation Performance of the Francis Turbine under Partial Flow Conditions. *Processes* **2021**, *9*, 1385. [CrossRef]
22. Zhou, Z. Numerical Study on the Blade Channel Vorticity in a Francis Turbine. *Fluid Dyn. Mater. Process.* **2021**, *17*, 1091–1100. [CrossRef]
23. Kan, K.; Zheng, Y.; Zhang, X.; Yang, C.; Zhang, Y. Numerical study on unidirectional fluid–solid coupling of Francis turbine runner. *Adv. Mech. Eng.* **2015**, *7*, 1687814015568938. [CrossRef]
24. Ji, L.; Xu, L.; Peng, Y.; Zhao, X.; Li, Z.; Tang, W.; Liu, D.; Liu, X. Experimental and Numerical Simulation Study on the Flow Characteristics of the Draft Tube in Francis Turbine. *Machines* **2022**, *10*, 230. [CrossRef]
25. Xie, L.; Du, Q.; Liu, G.; Lian, Z.; Xie, Y.; Luo, Y. Investigation of flow characteristics in a rotor-stator cavity under crossflow using wall-modelled large-eddy simulation. *J. Zhejiang Univ. Sci. A* **2023**, *24*, 473–496. [CrossRef]
26. Shang, L.; Cao, J.; Wang, L.; Yu, S.; Ding, S.; Wei, Z.; Wang, Z.; Liu, X. Analysis of Flow and Runner Dynamic Response Characteristics under Pump Conditions of Variable-Speed Pump Turbine. *J. Marine Sci. Eng.* **2023**, *11*, 1493. [CrossRef]

27. Zhang, J.; Zhu, Y.; Li, Y.; Huang, P.; Xu, H.; Zheng, F. Investigation of Unsteady Pressure Pulsation in New Type Dishwasher Pump with Special Double Tongue Volute. *Shock Vib.* **2022**, *2022*, 9349432. [CrossRef]
28. Gui, Z.; Xu, Z.; Li, D.; Zhang, F.; Zhao, Y.; Xu, L.; Zheng, Y.; Kan, K. Analysis of the Energy Loss Mechanism of Pump-Turbines with Splitter Blades under Different Characteristic Heads. *Water* **2013**, *15*, 2776. [CrossRef]
29. Kan, K.; Xu, Z.; Chen, H.; Xu, H.; Zheng, Y.; Zhou, D.; Muhirwa, A.; Maxime, B. Energy Loss Mechanisms of Transition from Pump Mode to Turbine Mode of an Axial-Flow Pump under Bidirectional Conditions. *Energy* **2022**, *257*, 124630. [CrossRef]
30. Yang, Z.; Cheng, Y.; Xia, L.; Meng, W.; Liu, K.; Zhang, X. Evolutions of flow patterns and pressure fluctuations in a prototype pump-turbine during the runaway transient process after pump-trip. *Renew. Energy* **2020**, *152*, 1149–1159. [CrossRef]